Electron density and electrostatic potential of KMnF$_3$: a phase-transition study

**Yury Ivanov,* Tatsuya Nimura
and Kiyoaki Tanaka**

Nagoya Institute of Technology, Gokiso-cho,
Showa-ku, Nagoya 466-8555, Japan

Correspondence e-mail: temples@rsl.ru

Three accurate X-ray diffraction experiments (Mo $K\alpha$, T = 190, 240 and 298 K) were carried out to track the temperature dependence of the electron density in the cubic perovskite potassium manganese trifluoride, KMnF$_3$, from room temperature to just above that of the phase transition to the tetragonal structure (186 K), and to correlate the parameters of the critical points with the phase-transition mechanism. The data obtained were approximated by the Hansen–Coppens multipole model expanded up to hexadecupoles; the anharmonicity of the atomic displacements up to the fourth level was considered. Topological analysis shows only two types of chemical bond at room temperature, Mn—F and K—F. However, at low temperature the K—F bonds blocking the rotation of the MnF$_6$ octahedra are weakened and new Mn—K bonds are formed to keep the crystal structure from disintegrating. The Mn—K bonds become stronger as the temperature approaches 186 K. This rearrangement of chemical bonds can be regarded as a precursor effect, which starts 50–60° above the phase-transition temperature. The effective one-particle potential of the F atom has a single minimum at 298 K and four well separated minima (with a shift of 0.2 Å from the equilibrium position towards the structural holes) at 190 K. Parameters of the critical points of the electron density indicate closed-shell type interactions between K—F and Mn—K pairs, whereas the Mn—F bond can be considered as an intermediate type. The topology of the electrostatic potentials is discussed as well.

1. Introduction

Perovskites are characterized by a wide variety of important physical properties (ferro-, antiferro-, piezo-electricity, dielectric susceptibility, superconductivity *etc*). Some of these properties are related to deviations from the basic cubic structure with $Pm\bar{3}m$ symmetry. The ideal cubic perovskites AMX_3 contain one formula per unit cell. The A and M cations are located at the sites with $m\bar{3}m$ point symmetry being coordinated by 12 and 6 X anions, respectively. Each X anion is in a distorted octahedron (at 4/*mmm*) of four A and two M cations. Distortions from the ideal structure can be described in terms of:

(i) displacements of A and M cations from the centers of their coordination polyhedra (AX_{12} and MX_6);

(ii) distortions of the anionic polyhedra;

(iii) tilting of the BX_6 octahedra about one, two or three axes.

Table 1
Experimental details.

	190 K	240 K	298 K
Crystal data			
Chemical formula	F_3MnK	F_3MnK	F_3MnK
M_r	151.03	151.03	151.03
Cell setting, space group	Cubic, $Pm\bar{3}m$	Cubic, $Pm\bar{3}m$	Cubic, $Pm\bar{3}m$
a (Å)	4.1850 (7)	4.1869 (5)	4.1893 (2)
V (Å^3)	73.30 (2)	73.40 (2)	73.52 (1)
Z	1	1	1
D_x (Mg m^{-3})	3.422	3.417	3.411
Radiation type	Mo $K\alpha$	Mo $K\alpha$	Mo $K\alpha$
No. of reflections for cell parameters	40	40	29
θ range (°)	68.5–72.0	68.3–71.9	68.3–71.9
μ (mm^{-1})	5.76	5.76	5.75
Temperature (K)	190 (1)	240 (1)	298 (1)
Crystal form, colour	Sphere, pale pink	Sphere, pale pink	Sphere, pale pink
Crystal radius (mm)	0.030	0.030	0.030
Data collection			
Diffractometer	Four-circle	Four-circle	Four-circle
Data collection method	Integrated intensities data from $\omega/2\theta$ scans	Integrated intensities data from $\omega/2\theta$ scans	Integrated intensities data from $\omega/2\theta$ scans
Absorption correction	For a sphere	For a sphere	For a sphere
T_{min}	0.772	0.772	0.772
T_{max}	0.780	0.780	0.780
No. of measured, independent and observed reflections	1058, 165, 165	1001, 156, 156	1145, 146, 146
Criterion for observed reflections	$F > 3.0\sigma(F)$	$F > 3.0\sigma(F)$	$F > 3.0\sigma(F)$
R_{int}	0.030	0.028	0.027
θ_{max} (°)	74.7	74.6	74.5
Range of h, k, l	$-9 \Rightarrow h \Rightarrow 11$	$-10 \Rightarrow h \Rightarrow 11$	$-5 \Rightarrow h \Rightarrow 11$
	$-9 \Rightarrow k \Rightarrow 11$	$-10 \Rightarrow k \Rightarrow 10$	$-11 \Rightarrow k \Rightarrow 11$
	$-7 \Rightarrow l \Rightarrow 10$	$-11 \Rightarrow l \Rightarrow 10$	$-8 \Rightarrow l \Rightarrow 11$
No. and frequency of standard reflections	3 every 30 reflections	3 every 30 reflections	3 every 30 reflections
Intensity decay (%)	No decay, variation 0.6	No decay, variation 0.6	No decay, variation 0.6
Refinement			
Refinement on	F	F	F
$R[F^2 > 2\sigma(F^2)]$, $wR(F^2)$, S	0.0060, 0.0086, 0.99	0.0064, 0.0090, 1.02	0.0053, 0.0071, 0.99
No. of reflections	165	156	146
No. of parameters	25	25	25
H-atom treatment	No H atoms present	No H atoms present	No H atoms present
Weighting scheme	$w = 1/[\sigma^2(F) + (0.007F)^2]$	$w = 1/[\sigma^2(F) + (0.007F)^2]$	$w = 1/[\sigma^2(F) + (0.005F)^2]$
$(\Delta/\sigma)_{max}$	<0.0001	<0.0001	<0.0001
$\Delta\rho_{max}$, $\Delta\rho_{min}$ (e Å^{-3})	1.90, −0.71	0.70, −0.41	0.92, −0.33
Extinction method	Becker–Coppens type 2 isotropic	Becker–Coppens type 2 isotropic	Becker–Coppens type 2 isotropic
Extinction coefficient	0.019 (7)	0.003 (7)	0.009 (5)

Computer programs used: *MXC* (MAC Science) and *IUANGLE* (Tanaka, 1994), *RSLC-3 UNICS* system (Sakurai & Kobayashi, 1979), *TDS*1&2 (Tsarkov & Tsirelson, 1991), *PROMETHEUS* (Zucker *et al.*, 1983), *MOLDOS*97 (Protas, 1997), *XPROP*98 (Ivanov *et al.*, 1997).

These deformations were investigated repeatedly both from the geometrical point of view (Megaw & Darlington, 1975; Glazer, 1975; Aleksandrov, 1976; O'Keeffe & Hyde, 1977; Deblieck *et al.*, 1985; Thomas, 1996, 1998; Howard & Stokes, 1998; Bock & Müller, 2002; Stokes *et al.*, 2002) and in its connection with the physical properties of perovskites (Schwabl, 1972, 1973; Rousseau, 1979; Kassan-Ogly & Naish, 1986a,b,c; Thomas, 1989; Thomas & Beitollahi, 1994; Woodward, 1997b; Magyari-Köpe *et al.*, 2001). The detailed classification of octahedral tilting in perovskites was made by Glazer (1972) and Woodward (1997a).

Correct understanding of the effects of structural distortions can be achieved only when the ideal case is fully investigated. The electron density (ED) distribution in cubic perovskites was studied many times by means of X-ray diffraction (mainly at room temperature; Kijima *et al.*, 1981, 1983; Miyata *et al.*, 1983; Buttner & Maslen, 1988, 1992; Maslen & Spadaccini, 1989; Maslen *et al.*, 1993, 1995; Abramov *et al.*, 1995; Zhurova *et al.*, 1995, 1999; Ikeda *et al.*, 1998; Takata *et al.*, 1999) and using *ab initio* calculations (Weyrich & Siems, 1985; Ricart *et al.*, 1995, 1997; Dovesi *et al.*, 1997; Luaña *et al.*, 1997). Several works devoted to the multipole analysis of the ED and the electrostatic potential in these crystals have been published recently (Sheu & Wang, 1998; Ivanov *et al.*, 1999; Tsirelson *et al.*, 2000; Zhurova, 2000; Zhurova *et al.*, 2000, 2001; Zhurova & Tsirelson, 2002).

Table 2
KMnF$_3$: harmonic and anharmonic displacement, and multipole model parameters.

The results are given in the sequence: 298, 240, 190 K from the top to the bottom.

	K ($\frac{1}{2}, \frac{1}{2}, \frac{1}{2}$)	Mn (0, 0, 0)	F ($\frac{1}{2}$, 0, 0)
U^{11} (Å^2)	0.01963 (7)	0.00756 (3)	0.0080 (3)
	0.01619 (7)	0.00631 (4)	0.0068 (2)
	0.01330 (5)	0.00525 (3)	0.0054 (2)
U^{22} (Å^2)	U^{11}	U^{11}	0.0340 (3)
			0.0313 (3)
			0.0304 (2)
$d_{1111} \times 10^4$ (Å^4)	−0.0006 (27)	0.0004 (14)	−0.0033 (16)
	0.0001 (15)	0.0005 (16)	−0.0003 (13)
	−0.0007 (19)	0.0001 (11)	−0.0017 (13)
$d_{2222} \times 10^4$ (Å^4)	d_{1111}	d_{1111}	−0.0083 (91)
			−0.0071 (65)
			−0.0154 (57)
$d_{1122} \times 10^4$ (Å^4)	−0.0047 (62)	−0.0019 (26)	0.0061 (94)
	−0.0095 (40)	−0.0014 (16)	−0.0073 (73)
	−0.0042 (40)	−0.0002 (26)	0.0017 (70)
$d_{2233} \times 10^4$ (Å^4)	d_{1122}	d_{1122}	−0.060 (14)
			−0.033 (15)
			−0.063 (12)
κ'	–	1.12 (2)	0.948 (4)
		1.13 (2)	0.957 (5)
		1.09 (2)	0.968 (5)
$\xi\kappa''$ (bohr^{-1})	1.4 (2)	3.6 (0.2)	8.4 (1.1)
	1.5 (3)	7.4 (0.7)	6.7 (1.7)
	1.6 (4)	12.0 (2.2)	3.8 (0.8)
P_v	0 (fixed)	6.35 (11)	7.55 (4)
		6.32 (12)	7.56 (4)
		6.48 (14)	7.51 (5)
P_{20}	–	–	−0.05 (3)
			−0.08 (3)
			−0.00 (3)
P_{40}	−0.36 (10)	0.31 (6)	0.12 (3)
	−0.46 (12)	0.14 (3)	0.05 (4)
	−0.30 (11)	0.11 (3)	0.13 (5)
P_{44+}	−0.27	0.23	0.06 (4)
	−0.34	0.10	0.03 (5)
	−0.22	0.09	0.16 (5)

The multi-temperature measurement of the ED of materials with interesting physical properties by X-ray diffraction provides information about the change in the nature of chemical bonds with temperature and the real reason for the characteristic property. The reason for the 4f-electron transfer in the Kondo crystal CeB$_6$ was revealed by the multi-temperature X-ray measurement of the ED (Tanaka & Onuki, 2002). The change in chemical bonds during a phase-transition process is a very interesting target for this method. The aim of the present study is to track the temperature dependence of the topology of the ED and thus of the chemical bonds in the cubic perovskite KMnF$_3$ from room temperature ($Pm\bar{3}m$ symmetry) to just above the phase tranistion at 186 K (to $I4/mcm$ symmetry). These weak first-order transitions, which corresponds to the alternate rotation of the MnF$_6$ octahedron about fourfold cubic axes, have been extensively studied previously using X-ray methods (*e.g.* Minkiewicz *et al.*, 1970; Nicholls & Cowley, 1987; Burandt *et al.*, 1994) and by means of other experimental techniques (*e.g.* Borsa, 1973; Gufan & Sadkov, 1979; Holt & Fossheim, 1981; Kapusta *et al.* 1999). The theoretical modeling was carried out by Lewis & Lépine (1989), Reiger *et al.* (1989) and Ratuszna & Kachel (1992).

Besides, the detailed theory of structural and magnetic phase transitions in the KMnF$_3$ crystal is presented by Konwent & Plakida (1983*a,b,c,d*).

2. Experimental

The pink single crystal of KMnF$_3$, synthesized using Bridge-mann's method, was used for three accurate X-ray diffraction experiments at 190, 240 and 298 K. The crystal was ground by the Bond method yielding a specimen of almost perfect spherical shape with a diameter of 60 μm. The measurements were carried out on a Mac Science diffractometer equipped with a molybdenum rotating anode and graphite mono-chromator (Mo $K\alpha$ radiation). The intensities of the reflections were measured in an $\omega/2\theta$ scan mode with a scan rate of $2°$ min^{-1}. The scan width was varied in accordance with $1.2 + 0.5\tan\theta$ (°). Three standard reflections (200, 020, 002) were measured every 30 reflections; the intensity variation did not exceed ±0.6% of the mean value. Multiple diffraction was avoided by the ψ-scan method (Tanaka *et al.*, 1994). The lattice parameters were determined over 40 (for 190 and 240 K) and over 29 (for 298 K) high-order reflections. The data sets were corrected for Lorentz and polarization factors, and for absorption. The correction for thermal diffuse scattering was carried out in the framework of the two-phonon approximation (Tsarkov & Tsirelson, 1991) using elastic constants from Hellwege (1979). Other experimental details are given in Table 1.

3. Refinement

The total ED of the crystal was approximated by the multipole (up to hexadecapole) model of Hansen & Coppens (1978) as the sum of the pseudoatomic electron densities, which are defined as

$$\rho_{\text{pseudoat}}(\mathbf{r}) = \rho_{\text{core}}(r) + P_{\text{val}}\kappa'^3\rho_{\text{val}}(\kappa' r)$$
$$+ \sum_{l=1}^{4} \kappa''^3 R_l(\kappa'' r) \sum_{m=-l}^{l} P_{lm} y_{lm}(\mathbf{r}/r).$$

The exponential radial functions $R_l(\kappa'' r) = r^{n_l}\exp(-\kappa''\xi r)$ with $n_4 = 8$ (for K, Mn) and with $n_2 = 2$, $n_4 = 4$ (for F) were used. Initial values for the orbital exponent coefficients $\xi_K = 1.65$, $\xi_{Mn} = 5.0$, $\xi_F = 5.1$ bohr^{-1} were selected in accordance with Clementi & Raimondi (1963). The neutral-atom wavefunctions by Clementi & Roetti (1974) were used to calculate the core and valence form factors. Anomalous dispersion coefficients were taken from the *International Tables for Crystallography* (1995). The anharmonicity of the atomic displacements was considered up to the fourth level using the Gram–Charlier expansion (*International Tables for Crystallography*, 1995). Refinements were carried out applying the program *MOLDOS*97 (Protas, 1997; Hansen & Coppens, 1978). The optimized parameters were: the scale factor, valence-shell populations P_{val} for Mn and F atoms, multipole populations P_{lm}, contraction–expansion coefficients κ' and κ'', and atomic displacement parameters. The lowest agreement
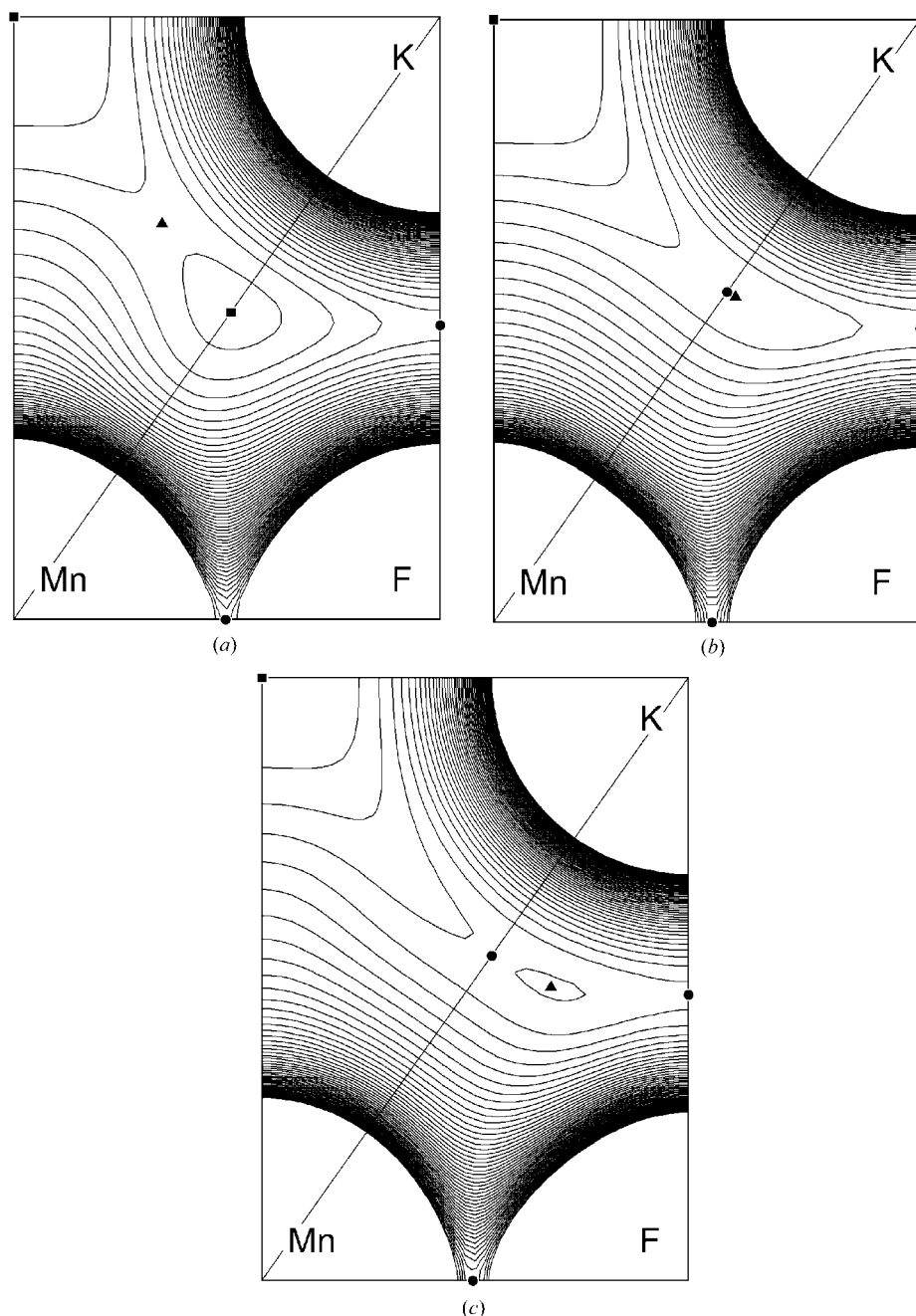
Figure 1
Static model of the total electron density in the (110) plane of $KMnF_3$ at (*a*) 298, (*b*) 240 and (*c*) 190 K. Contour interval: 0.01 e $Å^{-3}$. The critical points of the electron density are denoted as follows: filled circles: (3,−1), bond; filled triangles: (3,+1), ring; filled square: (3,+3), cage.

parameter and harmonic displacement parameters were fitted over all the data. Then, harmonic and anharmonic displacements were refined using only high-order reflections with $\sin\theta/\lambda \geq 0.7$ Å. Thereafter, the scale factor, extinction parameter and ED parameters κ', κ'', P_{val} and P_{lm} were refined using all the reflections. Finally, all the displacement parameters were again fitted over the high-order region and multipole parameters were then refined again over all data. The weighting schemes, used for calculations, are described in Table 1. The highest extinction effect was observed for 002 at 190 K. The intensity of this reflection was attenuated by only 4%. The correctness of the final results was inspected by a test as given in Abrahams & Keve (1971). It is necessary to point out that the multipole and anharmonic displacement parameters were refined separately using different data regions. At the last stage the test refinements were carried out and all the parameters were fitted over all the data sets. All correlation coefficients between multipole parameters and anharmonic displacement parameters were less than 0.6. So, an asphericity of valence electron shells and the anharmonicity of the atomic displacements are satisfactorily separated in our refinement. The final harmonic and anharmonic displacement, and multipole model parameters are reported in Table 2. The observed (F_{obs}) and calculated (F_{calc}) structure factors have been deposited.[1]

4. Results and discussion

The multipole parameters obtained were used to calculate the ED distribution maps and to obtain the parameters of the critical points (CPs). All the calculations were carried out using the program *XPROP*98 (Ivanov *et al.*, 1997). Both the Poincaré–Hopf–Morse relationship (Zou & Bader, 1994) and Euler's relationship for atomic basins (Martín Pendás *et al.*, 1997; Luaña *et al.*, 1997) have been analyzed to make sure that all CPs were found. The

factors were found when the K atom was approximated by an ionic scattering curve. Therefore, the valence population of potassium P_{val} was fixed at zero. The isotropic secondary extinction was corrected in accordance with the model of Becker & Coppens (1974). The electroneutrality condition was imposed on the unit cell during refinement.

The refinement procedure, based on $|F|$, was the same for all the experimental data sets. At first, the scale factor, extinction

Table 3
Parameters of the critical points in KMnF₃.

Type	Position	Bond	x	y	z	ρ (e Å⁻³)	$\nabla^2\rho$ (e Å⁻⁵)	λ_1 (e Å⁻⁵)	λ_2 (e Å⁻⁵)	λ_3 (e Å⁻⁵)	$\varepsilon = \lambda_1/\lambda_2$ − 1	$|\lambda_1|/\lambda_3$	h_e (a.u.)
298 K													
(3,−1)	(x, 0, 0)	Mn−F	0.248 (2)	0	0	0.48 (3)	5.9 (7)	−2.5 (3)	−2.5 (3)	11.0 (5)	0	0.23	−0.015 (3)
(3,−1)	($\frac{1}{2}$, y, y)	K−F	1/2	0.244 (2)	0.244 (2)	0.046 (5)	1.04 (6)	−0.17 (2)	−0.15 (2)	1.37 (8)	0.16	0.12	0.0029 (9)
(3,+1)	(x, x, z)		0.329 (10)	0.329 (10)	0.175 (14)	0.021 (4)	0.50 (5)	−0.08 (1)	0.21 (3)	0.37 (4)			
(3,+3)	(x, x, x)		0.256 (9)	0.256 (9)	0.256 (9)	0.016 (5)	0.50 (8)	0.13 (4)	0.13 (4)	0.23 (6)			
(3,+3)	(0, $\frac{1}{2}$, $\frac{1}{2}$)		0	1/2	1/2	0.000 (6)	0.17 (4)	0.04 (1)	0.06 (1)	0.06 (1)			
240 K													
(3,−1)	(x, 0, 0)	Mn−F	0.256 (2)	0	0	0.46 (3)	7.7 (7)	−2.6 (3)	−2.6 (3)	12.8 (6)	0	0.20	−0.006 (2)
(3,−1)	($\frac{1}{2}$, y, y)	K−F	1/2	0.244 (1)	0.244 (1)	0.044 (4)	1.05 (3)	−0.18 (3)	−0.10 (2)	1.34 (3)	0.72	0.13	0.0030 (7)
(3,−1)	(x, x, x)	Mn−K	0.276 (2)	0.276 (2)	0.276 (2)	0.031 (4)	0.52 (4)	−0.005 (20)	−0.005 (20)	0.53 (4)	0	0.01	0.0015 (4)
(3,+1)	(x, x, z)		0.272 (2)	0.272 (2)	0.284 (6)	0.031 (3)	0.52 (4)	−0.014 (20)	0.005 (20)	0.53 (4)			
(3,+3)	(0, $\frac{1}{2}$, $\frac{1}{2}$)		0	1/2	1/2	0.00 (1)	0.20 (8)	0.05 (3)	0.08 (3)	0.08 (3)			
190 K													
(3,−1)	(x, 0, 0)	Mn−F	0.247 (3)	0	0	0.46 (3)	7.1 (9)	−2.6 (4)	−2.6 (4)	12.3 (8)	0	0.21	−0.008 (3)
(3,−1)	($\frac{1}{2}$, y, y)	K−F	1/2	0.236 (4)	0.236 (4)	0.037 (9)	1.02 (12)	−0.10 (5)	−0.01 (9)	1.13 (9)	12.6	0.09	0.0030 (11)
(3,−1)	(x, x, x)	Mn−K	0.271 (4)	0.271 (4)	0.271 (4)	0.030 (9)	0.40 (8)	−0.03 (3)	−0.03 (3)	0.46 (4)	0	0.07	0.0010 (5)
(3,+1)	(x, x, z)		0.242 (10)	0.242 (10)	0.343 (31)	0.029 (8)	0.51 (10)	−0.02 (5)	0.05 (3)	0.47 (9)			
(3,+3)	(0, $\frac{1}{2}$, $\frac{1}{2}$)		0	1/2	1/2	0.00 (2)	0.27 (10)	0.04 (5)	0.11 (4)	0.11 (4)			

ED maps in the (110) section, which include all the symmetrically non-equivalent CPs, are presented in Fig. 1 and parameters of these CPs are reported in Table 3. The ED distribution at 298 K (Fig. 1*a*) exhibits two bond CPs: at the Mn—F and K—F lines, two minima (cage CPs), namely at the structural hole (0, $\frac{1}{2}$, $\frac{1}{2}$) and at the Mn—K line, and one ring CP between these minima. This pattern of CPs totally coincides with the topological schemes discovered earlier for KNiF₃ at room temperature (Ivanov *et al.*, 1999; Tsirelson *et al.*, 2000) and for KTaO₃ at room temperature (Zhurova *et al.*, 2000). The same scheme was also recently reported for both the theoretical and experimental (at 145 K) EDs of SrTiO₃ crystals (Zhurova & Tsirelson, 2002). At the same time, the ED distribution below 240 K exhibits an important change (Figs. 1*b* and *c*). The (3,+3) cage CP on the threefold axis passing through Mn and K atoms disappears and the (3,−1) bond CP is newly found below 240 K, while the (3,+1) ring CP on the (110) plane moves from the face-center side to the K—F bond side across the threefold axis. At 240 K the (3,−1) and (3,+1) CPs are very close to each other (0.04 Å), whereas at 190 K they are 0.35 Å apart. The larger separation at low temperature is also reflected by the higher absolute values of steep (λ_1) and soft (λ_2) curvatures of the ED at the corresponding CPs (see Table 3). Since the relative errors of the curvatures at CPs are large enough, and the type of CP depends only on the arithmetic signs of λs, the statistical significances of these patterns were checked by the Monte-Carlo method. The ED parameters obtained were varied statistically, taking into account their errors, and for each variation the redetermination of the topology of the ED was carried out. The ratio of the number of identical topological schemes to the full number of tests is the estimation of the significance of this topological scheme. It was found that the significance of the existence of the (3,+ 3) cage CP on the Mn—K line at room temperature is practically 100%, whereas the significance of the (3,−1) bond CP at the same position is equal to 56% at 240 K and reaches

87% at 190 K. On the other hand, the pattern of the CP demonstrates a high stability against variation in the refinement procedure. It should be mentioned that the comprehensive topological analysis of the ED of the cubic alkali-halide perovskites was carried out theoretically by Luaña *et al.* (1997). After analyzing 120 structures they found that the ED can be classified into one of seven different topological schemes in accordance with the type and location of its critical points (CPs). At the same time, some numerical experiments relative to the sizes of atoms were allowed to generate a rather large number of such schemes. Thus, the physical limitation of the ionic sizes effectively reduces the possible topological schemes. The pattern of CPs in KMnF₃ at 298 K (Fig. 1*a*) corresponds to the C_8(3212) scheme in Luaña *et al.*'s (1997) notation, whereas the authors have found no analogous bond as we observed for 240 and 190 K (Figs. 1*b* and *c*). Furthermore, Luaña *et al.* (1997) have discovered that the ratios of the topological radii along the *M*—*X* and *A*—*X* bond paths completely determine the topological scheme exhibited by the crystal. The ratios of the bonded radii (distances from equilibrium positions of nuclei to bond CPs), $R(MnF)/R(F{\rightarrow}Mn)$ and $R(K{\rightarrow}F)/R(F{\rightarrow}K)$, calculated from the parameters of the CPs of KMnF₃ (Table 4), correspond to the same C_8(3212) scheme for all three temperatures. These facts lead to an idea that the *M*—*A* (Mn—K) interaction appears exclusively in connection with the phase transition at 186 K. The CP on the Mn—K line is fixed by symmetry (Martín Pendás *et al.*, 1997) and in this case $\lambda_1 = \lambda_2$. Transformation of the (3,+3) cage CP with three positive curvatures to the (3,−1) bond CP requires an intermediate degenerate (1,+1) CP of rank 1 with $\lambda_1 = \lambda_2 = 0$. In Fig. 1(*b*) one can see a moment just after the splitting of this unstable point into a pair of bonds and ring CPs. Actually λ_1 and λ_2 of the bond CP at 240 K are equal at −0.005, which is very close to 0 (Table 3). Therefore, this splitting and nascence of the bond CP at the Mn—K line can be regarded as a *precursor* effect, which appears at around 240 K, 50–60° above
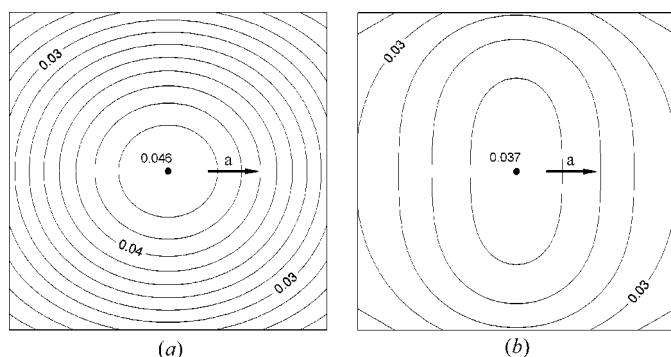
Table 4
Topological atomic radii derived from the total electron density (Bader's radii) and derived from the electrostatic potential (ESP).

Bond	Bader's radii (Å)			ESP radii (Å)		
	298 K	240 K	190 K	298 K	240 K	190 K
K−K	–	–	–	2.095 (= a/2)	2.093 (= a/2)	2.092 (= a/2)
K−Mn	–	1.63 (2)	1.66 (3)	1.92 (5)	1.95 (5)	1.93 (6)
K−F	1.52 (1)	1.52 (1)	1.56 (2)	1.95 (3)	1.94 (3)	1.92 (4)
Mn−K	–	2.00 (2)	1.97 (3)	1.71 (5)	1.68 (5)	1.69 (6)
Mn−F	1.03 (1)	1.07 (1)	1.05 (1)	1.25 (2)	1.23 (2)	1.24 (2)
F−K	1.44 (1)	1.44 (1)	1.40 (2)	1.01 (3)	1.02 (3)	1.04 (4)
F−Mn	1.07 (1)	1.02 (1)	1.05 (1)	0.85 (2)	0.86 (2)	0.85 (2)

the phase-transition temperature, mirroring not a quantitative but a qualitative change of the system. It is therefore concluded that a new very long (3.63 Å) Mn−K bond forms and the topological coordination numbers become 20 and 14 for K and Mn, respectively, in contrast with the numbers 12 and 6 at room temperature. The rearrangement of the chemical bonds or the *topological isomerization* far from the transition point was found theoretically by Martín Pendás *et al.* (1998) and at the phase transition by Blanco *et al.* (2000), both on alkali halides.

Another remarkable feature of the ED distribution at low temperature, as disclosed by the topological analysis, is the weakening of the K−F bond. This weakening manifests itself as a sharp growth of the bond ellipticity at 190 K, as shown in Fig. 2, and evaluated in terms of $\varepsilon = \lambda_1/_2 - 1$ in Table 3. The negative value of the soft curvature, λ_2, systematically increases to almost zero at 190 K, indicating that the K−F bond will be destroyed by changing the sign of λ_2, which will cause the switch of the CP type from (3,−1) to (3,+1). In such a case new CPs have to arise in the neighborhood of this point in order to keep both the Poincaré–Hopf–Morse and Euler relationships. The statistical significance of the bond CP on the K−F line is reduced from 100% at 298 and 240 K to 61% at 190 K, confirming the considerable decay of this bonding. Thus, at lower temperature the formation and strengthening (in terms of ED curvatures) of a new Mn−K bond and weakening of a K−F interaction are simultaneously observed

(Table 3), while the Mn−F bond remains virtually invariant. Although the shortest K−F and F−F distances are equal, there are no suggestions regarding the potential of the halogen–halogen (F−F) bond, which were found theoretically for many perovskites (Luaña *et al.*, 1997). Thereby, the main feature of the manganese atom basin, namely the triangular wings, which are wedged between F atoms and prevent the bond formation, are unchanged at the three temperatures. The existence of these wings was forecasted theoretically by Luaña *et al.* (1997) (see Fig. 3 in mentioned paper) and then affirmed experimentally for KNiF$_3$ (Tsirelson *et al.*, 2000), KTaO$_3$ (Zhurova, 2000; Zhurova *et al.*, 2000) and SrTiO$_3$ (Zhurova & Tsirelson, 2002). The change of the Mn basin shape is connected with the formation of new faces associated with new symmetry-equivalent bond CPs at Mn−K lines.

The classification of the chemical bonds in KMnF$_3$, especially the Mn−K interactions, is very interesting. It is known

(a)

(b)

Figure 3
The distributions of the effective one-particle atomic displacement potentials of the F atoms in the (200) plane of KMnF$_3$ crystals at (a) 298 and (b) 190 K. Contour interval: 0.5 meV.
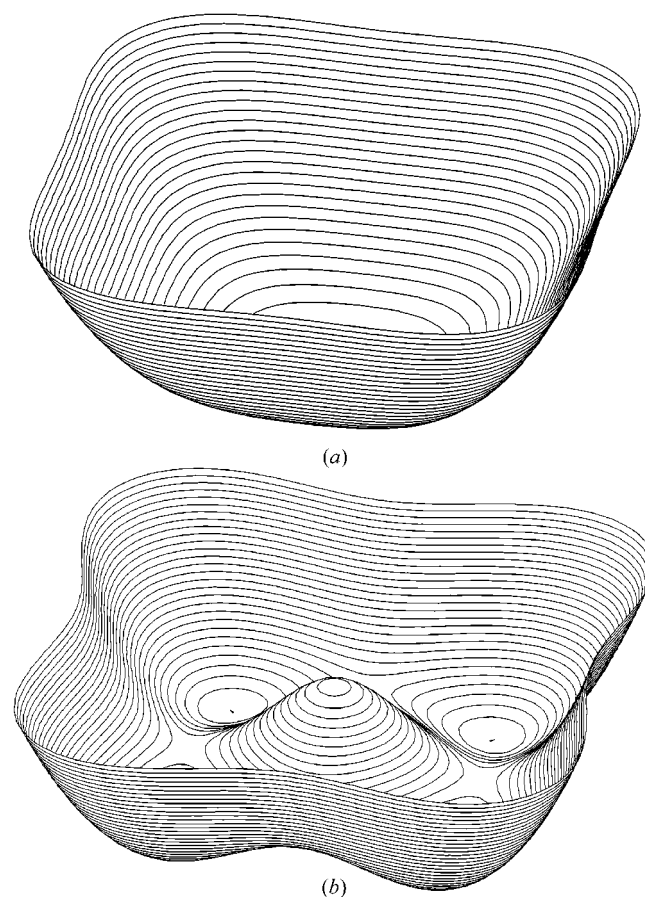

(a)

(b)

Figure 2
Electron density in the plane perpendicular to the K−F line and containing the bond critical point at (a) 298 and (b) 190 K. Contour interval: 0.002 e Å^{-3}. The bond critical points are in the center of the maps.

that the conventional description of these bonds as ionic is not enough to interpret the properties of perovskites (Megaw, 1952). According to Bader (1990), the low ED and positive value of the Laplacian ED at the bond CP correspond to the closed-shell interaction between a pair of atoms. However, in our case the values of $\rho(\mathbf{r}_{cp})$ and $\nabla^2\rho(\mathbf{r}_{cp})$ are insufficient to classify these bonds. Additional information can be obtained from the ratios of the first and third curvatures of the ED at the bond CPs. Analyzing the literature data, Tsirelson (1999) found that the $(3,-1)$ CPs at bonds, usually described as ionic, are characterized by two important relationships, $0.07 < \rho(\mathbf{r}_{cp}) < 0.25$ e Å^{-3} and $0.12 < |\lambda_1|/\lambda_3 < 0.17$. Analysis of the kinetic electronic energy density, $g(\mathbf{r})$, potential electronic energy density, $v(\mathbf{r})$, and density of the total electronic energy, $h_e(\mathbf{r}) = g(\mathbf{r}) + v(\mathbf{r})$ (Bader & Beddall, 1972), gives us an alternative gauge to classify the atomic interactions. According to Cremer & Kraka (1984), at the bond CP $h_e(\mathbf{r}_{cp}) > 0$ in the case of closed-shell interactions and $h_e(\mathbf{r}_{cp}) < 0$ in the case of shared (covalent) interactions. All the above-mentioned values are consolidated in Table 3. The fact that the gradient expansion given by Kirzhnits (1957) is more adequate than Yang's (1986) mean-path approximation (Tsirelson, 2002) was used to calculate $g(\mathbf{r})$. The potential electronic energy density was calculated *via* the local form of the virial theorem $2g(\mathbf{r}) + v(\mathbf{r}) = \frac{1}{4}\nabla^2\rho(\mathbf{r})$ (Bader & Beddall, 1972; Bader, 1990; Tsirelson, 2002). From these four criteria the conclusion can be made that KMnF$_3$ indicates closed-shell (ionic) type interactions in K—F and Mn—K pairs, whereas the Mn—F bond can be considered to be of intermediate type. The similar characteristics of the $M-X$ and $A-X$ bonds were recently identified for the cubic perovskites KNiF$_3$ (Tsirelson *et al.*, 2000), KTaO$_3$

(Zhurova, 2000; Zhurova *et al.*, 2000) and SrTiO$_3$ (Abramov *et al.*, 1995; Ikeda *et al.*, 1998; Takata *et al.*, 1999; Zhurova & Tsirelson, 2002); for the latter crystal an analysis of the electronic energy distributions was also carried out (Zhurova & Tsirelson, 2002).

Analysis of the anharmonicity of the atomic displacements of the F atom was carried out in terms of the effective one-particle atomic displacement potential (OPP). This potential is used in phenomenological models of the ferroelectric phase transitions. The OPP is connected to the probability density function (PDF) by the formula $V(\mathbf{r}) = -kT\ln[p(\mathbf{r})/p_{max}]$, where p_{max} is the maximal value of the PDF in a given space (Zucker & Schulz, 1982). The distributions of the OPP at 298 and 190 K are presented in Fig. 3. The F atom oscillates predominantly in the (200) plane; the OPP has single minimum at 298 K and four well separated minima (with the shift of 0.2 Å from equilibrium positions towards structural holes) at 190 K. In the last case the value of the PDF at the minima is 1.8 times higher than that at a central position. The intermediate picture at 240 K is a little more complex. Apart from the four minima in the (200) plane, there are two additional minima in the direction towards the Mn atoms. However, we are inclined to attribute this phenomenon to a data defect. The higher values of the figures-of-merit at 240 K confirm this supposition indirectly. Significant anharmonicity in KMnF$_3$ was also observed by Shevyrev *et al.* (1980), Hutton & Nelmes (1981) and Lehner *et al.* (1982, 1983). In the first two papers it was reported that the anharmonicity intensified at lower temperatures. In the present study a clear picture of the phase transition at 186 K is discovered. At lower temperatures the anharmonicity of the F atom becomes stronger and the atom delocalizes in a four-minima potential well statistically. The weakening of the K—F bonds and strengthening of the newly formed Mn—K bonds enable the rotation of regular MnF$_6$ octahedra around one of the F—Mn—F fourfold axes, keeping the framework of the Mn and K atoms. As was expected, the Mn—F bonds do not undergo noticeable changes. Above the temperature of the phase transition to the structure with $I4/mcm$ symmetry, the F atoms are expected to be frozen near the potential well minima, although the position of the minima are not exactly the same as those at 190 K. It should be noted that the 0.20 Å shift of the potential well minima at 190 K corresponds to a 5.5° rotation of the MnF$_6$ octahedron; this value is approximately twice the published experimental results (see Table 5). On the other hand, virtually the same shift (0.2 Å) can be seen on the PDF maps reported by Hutton & Nelmes (1981). Besides, the *ab initio* periodic Hartree–Fock calculation gives the optimal value of 6.32° in tetragonal geometry (Dovesi *et al.*, 1997).

It is instructive to compare our result with the ED picture in SrTiO$_3$, which exhibits a similar (Minkiewicz *et al.*, 1970; Hirotsu & Sawada, 1973; Hayward *et al.*, 2000) phase transition at 105 K. Ikeda *et al.* (1998) and Takata *et al.* (1999) applied the maximum entropy method to obtain the ED distribution in this crystal from the X-ray diffraction data at room temperature and at 70 K. It was found that no significant change in chemical bonding occurs through the phase transi-
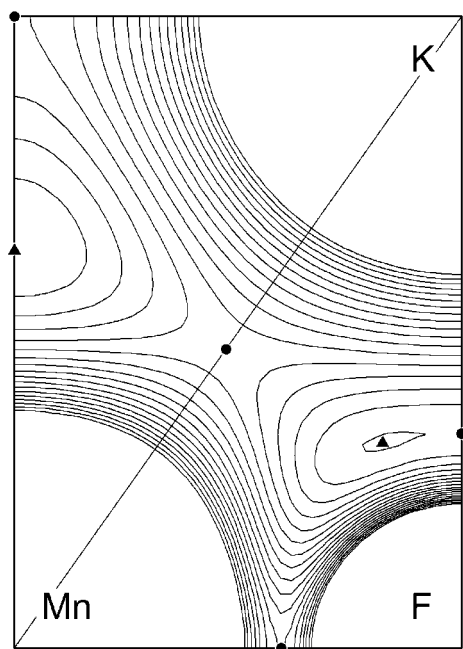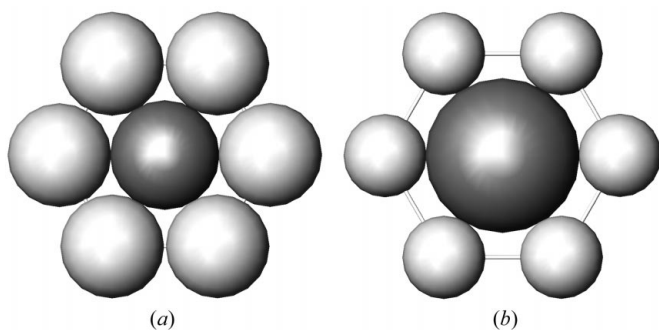

Figure 4
Electrostatic potential on the (110) plane of KMnF$_3$ at 298 K. Contour interval: 0.025 e Å^{-1}.

Table 5
Experimental values of the rotation angle of MnF$_6$ octahedron (°).

Physical method	Magnitude of discontinuity at the transition point	Angle at different temperatures	Reference
X-ray scattering		9.1 (145 K)	Minkiewicz et al. (1970)
Birefringence measurements	2.8	9.1 (145 K)	Hirotsu & Sawada (1973)
	3.18		Benard & Walker (1976)
Nuclear magnetic resonance		8 (120 K)	Borsa (1973)
Raman scattering	3.6		Bruce et al. (1980)
High-angle double-crystal X-ray diffractometry		2.63 (177 K)	Okazaki & Ono (1978)
		4.25 (139 K)	
		5.21 (100 K)	
	1.4	3.9 (150 K)	Kawaminami (1979)
(HADOX)	0.57 (single-well model)		Sakashita & Ohama (1982)
	0.70 (double-well model)		

tion. Unfortunately, the full topology of the ED was not discussed and the possibility of the formation of the Sr—Ti bond was not studied. As for anharmonicity, Abramov et al. (1995), using a high-precision X-ray diffraction technique, found, and Zhurova & Tsirelson (2002) confirmed (on the same data set), the anharmonic splitting of the oxygen position along the Ti—O—Ti line only. This picture strongly differs from our observations. Conversely, Hutton & Nelmes (1981), using elastic neutron-diffraction data at 112 and 293 K, Jauch & Palmer (1999), on the basis of γ-ray diffraction at 111 K, and Kiat et al. (2000), analyzing synchrotron and hot neutron diffraction multi-temperature data, found no anharmonicity in SrTiO$_3$. Furthermore, in the same work Hutton & Nelmes (1981) found significant anharmonicity in three other crystals investigated: KMnF$_3$, RbCaF$_3$ and CsPbCl$_3$. The disagreement between the KMnF$_3$ and SrTiO$_3$ results may be caused by the fact that the structural phase transition in KMnF$_3$ exhibits a weak first-order nature, in contrast to the second-order one in SrTiO$_3$ (Lockwood & Torrie, 1974; Sakashita et al., 1981; Nicholls & Cowley, 1987; Kapusta et al., 1999; Hayward et al., 2000).

The electrostatic potential (ESP) is also a very important inner-crystal scalar field, which attracts more and more attention. The ESP is defined to within a constant. In practice,

the evaluation of this constant involves some difficulties (Sommer-Larsen et al., 1990; Becker & Coppens, 1990; O'Keeffe & Spence, 1994). The optimal approach is therefore the analysis of the topology of the ESP, similar to the topological analysis of the ED. In our case the pattern of (3, −1) CPs does not depend on the temperature. These CPs were found on Mn—F, K—F, Mn—K and K—K lines (Fig. 4). Those of the first three correspond to the bond CPs in the ED (including the unusual Mn—K bond), whereas the fourth one appears on the same points, where the minimum of the ED exists. It is known that the ESP of the cation is a monotonically decreasing function, whereas the ESP of the anion has a minimum which is some distance from the nucleus (Sen & Politzer, 1989). The last peculiarity of the anion ESP led to the formation of a complicated distribution of (3, +1) and (3, −3) CPs around F atoms. Similar pictures of the ESP distribution were found recently for KNiF$_3$ (Tsirelson et al., 2000) and SrTiO$_3$ (Zhurova et al., 2001). The radii of K and Mn derived from the ESP are larger than those derived from the ED. The fluorine anions show the reverse picture (Table 4). Thus, in terms of ESP, the conventional concept of crystal structures (i.e. small cations in holes between large adjoining anions) is not justified (Spackman et al., 1987). The notion about a cationic grid as a basis of structure is more adequate here (Fig. 5). The role of the cationic matrix as a structure-forming factor was discussed recently by Vegas & Jansen (2002) for many classes of compounds.

Figure 5
A fragment of the K—F close-packed layer in the KMnF$_3$ structure. K atoms are in the centers of the pictures: (a) Bader's topological radii $R(K \rightarrow F)$ are used; (b) ESP's radii $R(K \rightarrow F)$ and $R(F \rightarrow K)$ are used.

References

Abrahams, S. C. & Keve, E. T. (1971). Acta Cryst. A**27**, 157–165.
Abramov, Yu. A., Tsirelson, V. G., Zavodnik, V. E., Ivanov, S. A. & Brown, I. D. (1995). Acta Cryst. B**51**, 942–951.
Aleksandrov, K. S. (1976). Ferroelectrics, **14**, 801–805.
Bader, R. F. W. (1990). Atoms in Molecules: a Quantum Theory. Oxford University Press.
Bader, R. F. W. & Beddall, P. M. (1972). J. Chem. Phys. **56**, 3320–3329.
Becker, P. & Coppens, P. (1974). Acta Cryst. A**30**, 129–147.
Becker, P. & Coppens, P. (1990). Acta Cryst. A**46**, 254–258.
Benard, D. J. & Walker, W. C. (1976). Rev. Sci. Instrum. **47**, 122–127.
Blanco, M. A., Costales, A., Martín Pendás, A. & Luaña, V. (2000). Phys. Rev. B, **62**, 12028–12039.
Bock, O. & Müller, U. (2002). Acta Cryst. B**58**, 594–606.
Borsa, F. (1973). Phys. Rev. B, **7**, 913–917.
Bruce, A. D., Taylor, W. & Murray, A. F. (1980). J. Phys. C Solid State Phys. **13**, 483–504.
Burandt, B., Rothaug, S. & Press, W. (1994). J. Phys. Condens. Matter, **6**, 7189–7198.
Buttner, R. H. & Maslen, E. N. (1988). Acta Cryst. C**44**, 1707–1709.
Buttner, R. H. & Maslen, E. N. (1992). Acta Cryst. B**48**, 639–644.

Clementi, E. & Raimondi, D. L. (1963). *J. Chem. Phys.* **38**, 2686–2689.

Clementi, E. & Roetti, C. (1974). *At. Data Nucl. Data Tables*, **14**, 177–478.

Cremer, D. & Kraka, E. (1984). *Croat. Chem. Acta*, **57**, 1259–1281.

Deblieck, R., Van Tendeloo, G., Van Landuyt, J. & Amelinckx, S. (1985). *Acta Cryst.* B**41**, 319–329.

Dovesi, R., Fava, F. F., Roetti, C. & Saunders, V. R. (1997). *Faraday Discuss.* **106**, 173–187.

Glazer, A. M. (1972). *Acta Cryst.* B**28**, 3384–3392.

Glazer, A. M. (1975). *Acta Cryst.* A**31**, 756–762.

Gufan, Yu. M. & Sadkov, A. N. (1979). *Sov. Phys. Solid State*, **21**, 1764–1768.

Hansen, N. K. & Coppens, P. (1978). *Acta Cryst.* A**34**, 909–921.

Hayward, S. A., Romero, F. J., Gallardo, M. C., del Cerro, J., Gibaud, A. & Salje, E. K. H. (2000). *J. Phys. Condens. Matter*, **12**, 1133–1142.

Hellwege, K.-H. (1979). Editor. *Landolt–Börnstein. Numerical Data and Functional Relationships in Science and Technology*, New Series, Group III, Vol. 11. Berlin: Springer-Verlag.

Hirotsu, S. & Sawada, S. (1973). *Solid State Commun.* **12**, 1003–1005.

Holt, R. M. & Fossheim, K. (1981). *Phys. Rev. B*, **24**, 2680–2692.

Howard, C. J. & Stokes, H. T. (1998). *Acta Cryst.* B**54**, 782–789.

Hutton, J. & Nelmes, R. J. (1981). *J. Phys. C Solid State Phys.* **14**, 1713–1736.

Ikeda, T., Kobayashi, T., Takata, M., Takayama, T. & Sakata, M. (1998). *Solid State Ion.* **108**, 151–157.

Ivanov, Yu., Abramov, Yu. & Tsirelson, V. (1997). *Natl Conf. on Application of the X-ray, Neutrons and Electrons for Study of Materials. Abstracts*, p. 599. Dubna: JINR.

Ivanov, Yu., Zhurova, E. A., Zhurov, V. V., Tanaka, K. & Tsirelson, V. G. (1999). *Acta Cryst.* B**55**, 923–930.

Jauch, W. & Palmer, A. (1999). *Phys. Rev. B*, **60**, 2961–2963.

Kapusta, J., Daniel, Ph. & Ratuszna, A. (1999). *Phys. Rev. B*, **59**, 14235–14245.

Kassan-Ogly, F. A. & Naish, V. E. (1986a). *Acta Cryst.* B**42**, 307–313.

Kassan-Ogly, F. A. & Naish, V. E. (1986b). *Acta Cryst.* B**42**, 314–325.

Kassan-Ogly, F. A. & Naish, V. E. (1986c). *Acta Cryst.* B**42**, 325–335.

Kawaminami, M. (1979). *Sci. Rep. Kagoshima University* **28**, 67–74.

Kiat, J.-M., Baldinozzi, G., Dunlop, M., Malibert, C., Dkhil, B., Ménoret, C., Masson, O. & Fernandez-Diaz, M.-T. (2000). *J. Phys. Condens. Matter*, **12**, 8411–8425.

Kijima, N., Tanaka, K. & Marumo, F. (1981). *Acta Cryst.* B**37**, 545–548.

Kijima, N., Tanaka, K. & Marumo, F. (1983). *Acta Cryst.* B**39**, 557–561.

Kirzhnits, D. A. (1957). *Sov. Phys. JETP*, **5**, 64–71.

Konwent, H. & Plakida, N. M. (1983a). *Acta Phys. Pol. A*, **63**, 755–768.

Konwent, H. & Plakida, N. M. (1983b). *Acta Phys. Pol. A*, **63**, 769–778.

Konwent, H. & Plakida, N. M. (1983c). *Acta Phys. Pol. A*, **63**, 779–790.

Konwent, H. & Plakida, N. M. (1983d). *Acta Phys. Pol. A*, **63**, 791–804.

Lehner, N., Rauh, H., Strobel, K., Geick, R., Heger, G., Bouillot, J., Renker, B., Rousseau, M. & Stirling, W. G. (1982). *J. Phys. C Solid State Phys.* **15**, 6545–6564.

Lehner, N., Rauh, H., Strobel, K., Geick, R., Heger, G., Bouillot, J., Renker, B., Rousseau, M. & Stirling, W. G. (1983). *J. Phys. C: Solid State Phys.* **16**, 3215.

Lewis, L. J. & Lépine, Y. (1989). *Phys. Rev. B*, **40**, 3319–3322.

Lockwood, D. J. & Torrie, B. H. (1974). *J. Phys. C Solid State Phys.* **7**, 2729–2744.

Luaña, V., Costales, A. & Martín Pendás, A. (1997). *Phys. Rev. B*, **55**, 4285–4297.

Magyari-Köpe, B., Vitos, L., Johansson, B. & Kollár, J. (2001). *Acta Cryst.* B**57**, 491–496.

Martín Pendás, A., Costales, A. & Luaña, V. (1997). *Phys. Rev. B*, **55**, 4275–4284.

Martín Pendás, A., Costales, A. & Luaña, V. (1998). *J. Phys. Chem. B*, **102**, 6937–6948.

Maslen, E. N. & Spadaccini, N. (1989). *Acta Cryst.* B**45**, 45–52.

Maslen, E. N., Spadaccini, N., Ito, T., Marumo, F. & Satow, Y. (1995). *Acta Cryst.* B**51**, 939–942.

Maslen, E. N., Spadaccini, N., Ito, T., Marumo, F., Tanaka, K. & Satow, Y. (1993). *Acta Cryst.* B**49**, 632–636.

Megaw, H. D. (1952). *Acta Cryst.* **5**, 739–749.

Megaw, H. D. & Darlington, C. N. W. (1975). *Acta Cryst.* A**31**, 161–173.

Minkiewicz, V. J., Fujii, Y. & Yamada, Y. (1970). *J. Phys. Soc. Jpn*, **28**, 443–450.

Miyata, N., Tanaka, K. & Marumo, F. (1983). *Acta Cryst.* B**39**, 561–564.

Nicholls, U. J. & Cowley, R. A. (1987). *J. Phys. C Solid State Phys.* **20**, 3417–3437.

Okazaki, A. & Ono, M. (1978). *J. Phys. Soc. Jpn*, **45**, 206–211.

O'Keeffe, M. & Hyde, B. G. (1977). *Acta Cryst.* B**33**, 3802–3813.

O'Keeffe, M. & Spence, J. C. H. (1994). *Acta Cryst.* A**50**, 33–45.

Protas, J. (1997). *MOLDOS*97. Private communication.

Ratuszna, A. & Kachel, A. (1992). *Acta Cryst.* B**48**, 118–122.

Reiger, R., Prade, J., Schröder, U., de Wette, F. W., Kulkarni, A. D. & Kress, W. (1989). *Phys. Rev. B*, **39**, 7938–7948.

Ricart, J. M., Dovesi, R., Roetti C. & Saunders, V. R. (1995). *Phys. Rev. B*, **52**, 2381–2389.

Ricart, J. M., Dovesi, R., Roetti C. & Saunders, V. R. (1997). *Phys. Rev. B*, **55**, 15942.

Rousseau, M. (1979). *J. Phys. Lett.* **40**, L-439–L-443.

Sakashita, H. & Ohama, N. (1982). *Phase Transit* **2**, 263–276.

Sakashita, H., Ohama, N. & Okazaki, A. (1981). *J. Phys. Soc. Jpn*, **50**, 4013–4021.

Sakurai, T. & Kobayashi, K. (1979). *Rep. Inst. Phys. Chem. Res.* **55**, 69–77.

Schwabl, F. (1972). *Phys. Rev. Lett.* **28**, 500–503.

Schwabl, F. (1973). *Phys. Rev. B*, **7**, 2038–2046.

Sen, K. D. & Politzer, P. (1989). *J. Chem. Phys.* **90**, 4370–4372.

Sheu, H.-S. & Wang, Y. (1998). *Proc. 41th Seminar on Science and Technology 'Crystallography'*, pp. 127–137. Osaka.

Shevyrev, A. A., Muradyan, L. A., Zavodnik, V. E., Aleksandrov, K. S. & Simonov, V. I. (1980). *Sov. Phys. Cryst.* **25**, 319–321.

Sommer-Larsen, P., Kadziola, A. & Gajhede, M. (1990). *Acta Cryst.* A**46**, 343–351.

Spackman, M. A., Hill, R. J. & Gibbs, G. V. (1987). *Phys. Chem. Miner.* **14**, 139–150.

Stokes, H. T., Kisi, E. H., Hatch, D. M. & Howard, C. J. (2002). *Acta Cryst.* B**58**, 934–938.

Takata, M., Ikeda, T., Nishibori, E., Kato, K. & Sakata, M. (1999). *Proc. Int. Conf. Solid-Solid Phase Transformations '99 (JIMIC-3)*, pp. 685–688.

Tanaka, K., Kumazawa, S., Tsubokawa, M., Maruno, S. & Shirotani, I. (1994). *Acta Cryst.* A**50**, 246–252.

Tanaka, K. & Onuki, Y. (2002). *Acta Cryst.* B**58**, 423–436.

Thomas, N. W. (1989). *Acta Cryst.* B**45**, 337–344.

Thomas, N. W. (1996). *Acta Cryst.* B**52**, 16–31.

Thomas, N. W. (1998). *Acta Cryst.* B**54**, 585–599.

Thomas, N. W. & Beitollahi, A. (1994). *Acta Cryst.* B**50**, 549–560.

Tsarkov, A. G. & Tsirelson, V. G. (1991). *Phys. Status Sol. B*, **167**, 417–428.

Tsirelson, V. G. (1999). *Acta Cryst.* A**55,** Supplement, Abstract M13.OF.003.

Tsirelson, V. G. (2002). *Acta Cryst.* B**58**, 632–639.

Tsirelson, V., Ivanov, Yu., Zhurova, E., Zhurov, V. & Tanaka, K. (2000). *Acta Cryst.* B**56**, 197–203.

Vegas, A. & Jansen, M. (2002). *Acta Cryst.* B**58**, 38–51.

Weyrich, K.-H. & Siems, R. (1985). *Z. Phys. B*, **61**, 63–68.

Woodward, P. M. (1997a). *Acta Cryst.* B**53**, 32–43.

Woodward, P. M. (1997b). *Acta Cryst.* B**53**, 44–66.

Yang, W. (1986). *Phys. Rev. A*, **34**, 4575–4585.

Zhurova, E. (2000). *Sagamore XIII. Conference on Charge, Spin and Momentum densities. Abstracts*, p. 43.

Zhurova, E. A., Ivanov, Yu., Zavodnik, V. & Tsirelson, V. (2000). *Acta Cryst.* B**56**, 594–600.

Zhurova, E. A. & Tsirelson, V. G. (2002). *Acta Cryst.* B**58**, 567–575.

Zhurova, E. A., Zavodnik, V. E. & Tsirelson, V. G. (1995). *Crystallogr. Rep.* **40**, 753–760.

Zhurova, E. A., Zhurov, V. V. & Tanaka, K. (1999). *Acta Cryst.* B**55**, 917–922.

Zhurova, E. A., Zuo, J. M. & Tsirelson, V. G. (2001). *J. Phys. Chem. Solids*, **62**, 2143–2146.

Zou, P. F. & Bader, R. F. W. (1994). *Acta Cryst.* A**50**, 714–725.

Zucker, U. H., Perenthaler, E., Kuhs, W. F., Bachmann, R. & Schulz, H. (1983). *J. Appl. Cryst.* **16**, 358.

Zucker, U. H. & Schulz, H. (1982). *Acta Cryst.* A**38**, 563–568.